



**HAL**  
open science

## Low velocity impact modeling in composite laminates capturing permanent indentation

Christophe Bouvet, Samuel Rivallant, Jean-Jacques Barrau

► **To cite this version:**

Christophe Bouvet, Samuel Rivallant, Jean-Jacques Barrau. Low velocity impact modeling in composite laminates capturing permanent indentation. *Composites Science and Technology*, 2012, 72 (16), pp.1977-1988. 10.1016/j.compscitech.2012.08.019 . hal-01853076

**HAL Id: hal-01853076**

**<https://hal.science/hal-01853076v1>**

Submitted on 2 Aug 2018

**HAL** is a multi-disciplinary open access archive for the deposit and dissemination of scientific research documents, whether they are published or not. The documents may come from teaching and research institutions in France or abroad, or from public or private research centers.

L'archive ouverte pluridisciplinaire **HAL**, est destinée au dépôt et à la diffusion de documents scientifiques de niveau recherche, publiés ou non, émanant des établissements d'enseignement et de recherche français ou étrangers, des laboratoires publics ou privés.



## Open Archive Toulouse Archive Ouverte (OATAO)

OATAO is an open access repository that collects the work of Toulouse researchers and makes it freely available over the web where possible.

This is an author-deposited version published in: <http://oatao.univ-toulouse.fr/>  
Eprints ID: 6769

**To link to this article:** DOI:10.1016/j.compositech.2012.08.019  
URL: <http://dx.doi.org/10.1016/j.compositech.2012.08.019>

**To cite this version:** Bouvet, Christophe and Rivallant, Samuel and Barrau, Jean-Jacques *Low velocity impact modeling in composite laminates capturing permanent indentation*. (2012) Composites Science and Technology, vol. 72 (n° 16). pp. 1977-1988. ISSN 0266-3538

Any correspondence concerning this service should be sent to the repository administrator: [staff-oatao@inp-toulouse.fr](mailto:staff-oatao@inp-toulouse.fr)

# Low velocity impact modeling in composite laminates capturing permanent indentation

C. Bouvet\*, S. Rivallant, J.J. Barrau

Université de Toulouse; INSA, UPS, Mines Albi, ISAE; ICA (Institut Clément Ader); ISAE, 10 Avenue Edouard Belin, 31055 Toulouse Cedex 4, France

## ARTICLE INFO

### Keywords:

B. Impact behavior  
C. Damage tolerance  
B. Delamination

## ABSTRACT

This paper deals with impact damage and permanent indentation modeling. A numerical model has been elaborated in order to simulate the different impact damage types developing during low velocity/low energy impact. The three current damage types: matrix cracking, fiber failure and delamination, are simulated. Inter-laminar damage, i.e. interface delamination, is conventionally simulated using interface elements based on fracture mechanics. Intra-laminar damage, i.e. matrix cracks, is simulated using interface elements based on failure criterion. Fiber failure is simulated using degradation in the volume elements. The originality of this model is to simulate permanent indentation after impact with a “plastic-like” model introduced in the matrix cracking elements. This model type is based on experimental observations showing matrix cracking debris which block crack closure. Lastly, experimental validation is performed, which demonstrates the model’s satisfactory relevance in simulating impact damage. This acceptable match between experiment and modeling confirms the interest of the novel approach proposed in this paper to describe the physics behind permanent indentation.

## 1. Introduction

Low velocity impact is one of the most critical load factors for composite laminates. Indeed, for structures submitted to low energy impacts or small dropped objects, such as tools during assembly or maintenance operations, composite laminates reveal a brittle behavior and can undergo significant damage in terms of matrix cracks, fiber breakage or delamination. This damage is particularly dangerous because it drastically reduces the residual mechanical characteristics of the structure, and at the same time can leave very limited visible marks on the impacted surface [1].

Consequently, it is essential to define a damage tolerance demonstration to design this type of structure in order to take possible damage into account. The damage tolerance concept [2] was introduced in the seventies for civil aircraft structures and these requirements are expressed by European certification JAR 25.571: “The damage tolerance evaluation of the structure is intended to ensure that should serious fatigue, corrosion or accidental damage occur within the operational life of the airplane, the remaining structure can withstand reasonable loads without failure or excessive structural deformation until the damage is detected”. In the field of aeronautics, damage tolerance, for damage corresponding to impact loading, leads to dimensioning the structure according to impact detectability: if the damage is not visibly detectable,

i.e. when the impact indentation depth is less than a given value, called barely visible impact damage (BVID), the structure must support extreme loads and if the damage is detectable, i.e. when the impact indentation depth is greater than BVID, another criterion must be considered, such as repair or replacement of the structure [2,3].

The BVID is defined as the minimum damage that can be detected by visual evaluation [2]. In the field of aeronautics, it has been demonstrated that a permanent indentation between 0.25 and 0.5 mm is detectable during detailed visual inspection with a probability greater than 99% [4].

Consequently, the development of numerical tools is essential to the aerospace industry to optimize composite structures according to the damage tolerance concept. Thus, the challenge is to simulate, with the same model, damage during impact and in particular permanent indentation, and the residual mechanical characteristics after impact, in order to be able to numerically optimize design of composite structures with impact damage tolerance. Many authors have studied the impact behavior of composite structures and its effect on residual strength, both experimentally (e.g. [1,5–7]), as well as numerically (e.g. [8–11]), and although some authors have worked on the permanent indentation phenomenon (e.g. [6,12–15]), considerable work is still necessary to understand the physics of this phenomenon and to correctly model it. Currently, this residual deformation after impact is explained, for thermoset resin such as epoxy, with “plasticity”. Indeed, this type of resin presents important permanent

\* Corresponding author.

E-mail address: christophe.bouvet@isae.fr (C. Bouvet).

deformation after testing, particularly under shear stress [16], similar to plasticity deformation. Consequently, some authors simulate this permanent indentation using plasticity modeling of the matrix (e.g. [17–19]). For example, Shi et al. [15] simulate damage development in a simple cross ply  $[0,90]_{25}$  in composite laminate subjected to low velocity impact and in particular permanent deformation after impact. A stress-based failure criterion was used to predict damage initiation while damage propagation in the form of intra- and inter-laminar cracking was simulated by energy based criteria. The permanent indentation is formed due to the modeling of the nonlinear shear behavior of the polymer matrix developed by Berbinau [20] (Fig. 1).

Another approach consists of using conventional Hertz contact modeling. For example, Karakuzu et al. [21] perform an experimental and numerical study of a glass/epoxy composite plate and empirically simulate the permanent indentation  $\alpha_0$  as:

$$\alpha_0 = \alpha_m \cdot (1 - (\alpha_{cr}/\alpha_m)^n) \quad (1)$$

where  $\alpha_m$  is the maximum indentation,  $\alpha_{cr}$  is a material parameter, corresponding to a critical indentation and  $n$  is a material parameter. This approach accurately reproduces the permanent indentation value, but does not make it possible to totally simulate the plate deformation after impact on the impacted and non-impacted sides. Another empirical approach is used by Caprino et al. [14]. In this study of indentation and penetration of carbon fiber reinforced plastic laminates, they predict the indentation as an empirical function of impact energy level. In practical terms, they show that a single indentation law function of impact energy level and penetration energy, holds for many laminates with different fiber architectures, laminate types, matrix types and constraint conditions. The drawback of this type of modeling is its inability to totally reproduce plate deformation because this model is totally linked to a test type, such as impact.

Recently, Gonzalez et al. [22] also proposed a model able to simulate impact and compression after impact (CAI) tests. This model uses constitutive material models formulated within the context of continuum damage mechanics and accounts for both ply failure mechanics and delamination. The comparisons with experimental data seem accurate, both for impact test, as well as for CAI, although insufficient knowledge of the real CAI damage obtained experimentally makes difficult these comparisons. However, permanent indentation is not taken into account. But this work is in progress

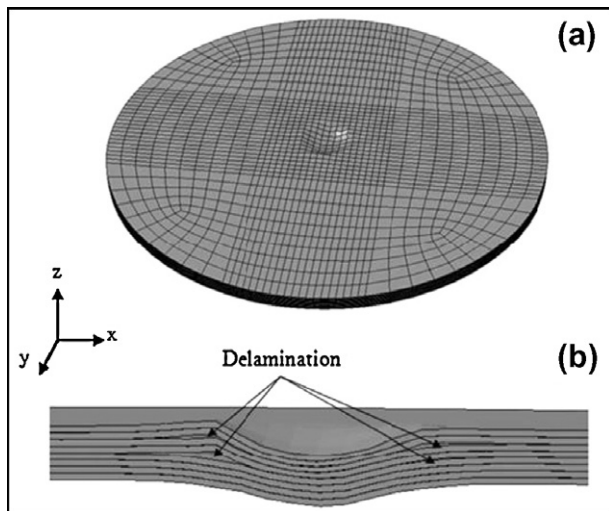


Fig. 1. Permanent indentation predicted by the numerical model of Shi et al. [15]: impacted side (a) and through the thickness (b).

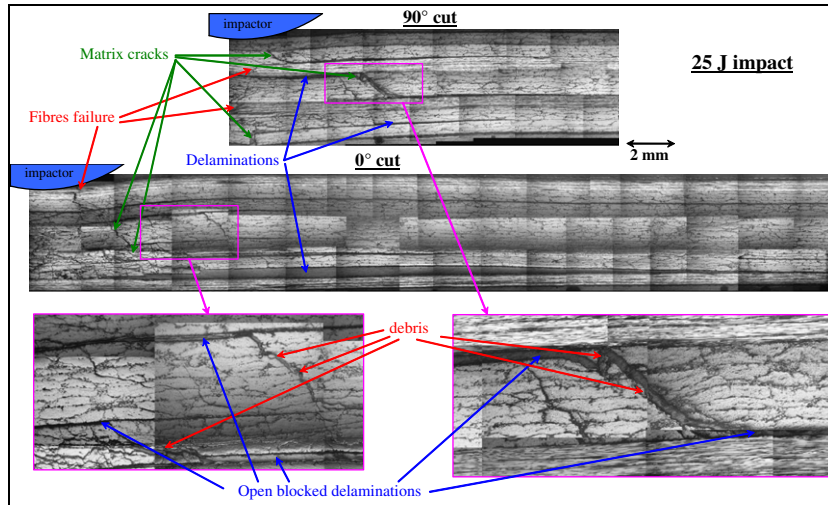
and the authors argue that using the coupled plasticity and damage model for in-plane and out-of-plane loading conditions of Donadon et al. [23] will make it possible to capture the permanent dent depth. The modeling developed by Faggiani and Falzon [17] is also able to simulate impact and CAI tests on a real structure. Faggiani and Falzon simulate impact damage and residual strength of a stiffened composite panel under compression. To do this, an intra-laminar damage model, based on continuum damage mechanics, is coupled with interface elements, based on the critical energy release rate. The permanent indentation after impact of the panel is simulated using nonlinear shear formulation of the intra-laminar damage model. Faggiani and Falzon observe that this deformation should be significant in predicting the CAI response of the panel. The numerical correlation on time-force history, on damage shape and on residual strength correlates satisfactorily. Nevertheless, insufficient knowledge of the real impact damage obtained experimentally makes it difficult to evaluate the reliability of this model. In particular, the ultrasonic investigations (C-Scan) given in this study are not experimentally reproducible to determine the delaminated interface shapes and other experimental examinations, such as micrographic cuts or subsequent image inter-correlation during CAI tests, are needed to evaluate the reliability of the model. However, this conclusion is generally valid for many models in the literature and experimental investigations of impact tests are often insufficient to evaluate the domain of their validity.

This conclusion is also valid for the physical phenomenon responsible for permanent indentation. Although resin plasticity is conventionally admitted as an explanation for this residual deformation, other phenomena may play a role. For example, Chen et al. [13] studied failure mechanisms of laminated composites subjected to static indentation and showed an apparent coupling between permanent indentation and fiber failure. In practical terms, the transition of rapid increase in dent depth is due to fiber failure produced at the impact force plateau. This coupling is not easy to explain using only resin plasticity, and other failure phenomena should create permanent indentation. In a previous study [24], we suggested that another phenomenon responsible for permanent deformation seems to be impact debris in  $45^\circ$  cracks through the ply thickness (Fig. 2a). Indeed, in these photographs, taken after a 25 J impact test on a composite laminate with unidirectional (UD) reinforcement (cf. Section 3), debris in the  $45^\circ$  matrix cracks seem to block their closure and to hold the adjacent delaminations open. This phenomenon is schematically presented in Fig. 2b and could explain part of the permanent indentation phenomenon. Nevertheless, it cannot fully explain permanent indentation and other phenomena, such as plasticity or compaction of the resin (due to initial porosity) or friction of delaminated interfaces, matrix cracks or fiber/resin debonding, may play a role.

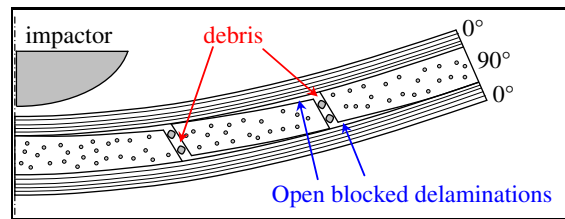
Lastly, the goal and the originality of this study is to propose a numerical model which is able to represent permanent indentation taking into account this phenomenon of debris blocking the matrix cracks closure. The model presented consists of an evolution based on a previous version [24,25] with integration of permanent indentation and modification of the fiber failure criterion.

The first section (Section 2) presents the basic approach for modeling the three most common damage types developed during impact: matrix cracking, delamination and fiber failures. Permanent indentation is simulated using an original “plastic-like” model introduced in the matrix cracking interfaces.

Section 3 deals with experimental validation. An impact reference case has been chosen to evaluate the accuracy of the proposed model. Then, this model is used to highlight some experimental results, such as the formation of delamination of the first interface on the non-impacted side, or the residual shape of the plate on impacted and non-impacted sides.



(a)



(b)

Fig. 2. Micrographic cuts after 25 J impact (a) and the principle of creation of permanent indentation (b).

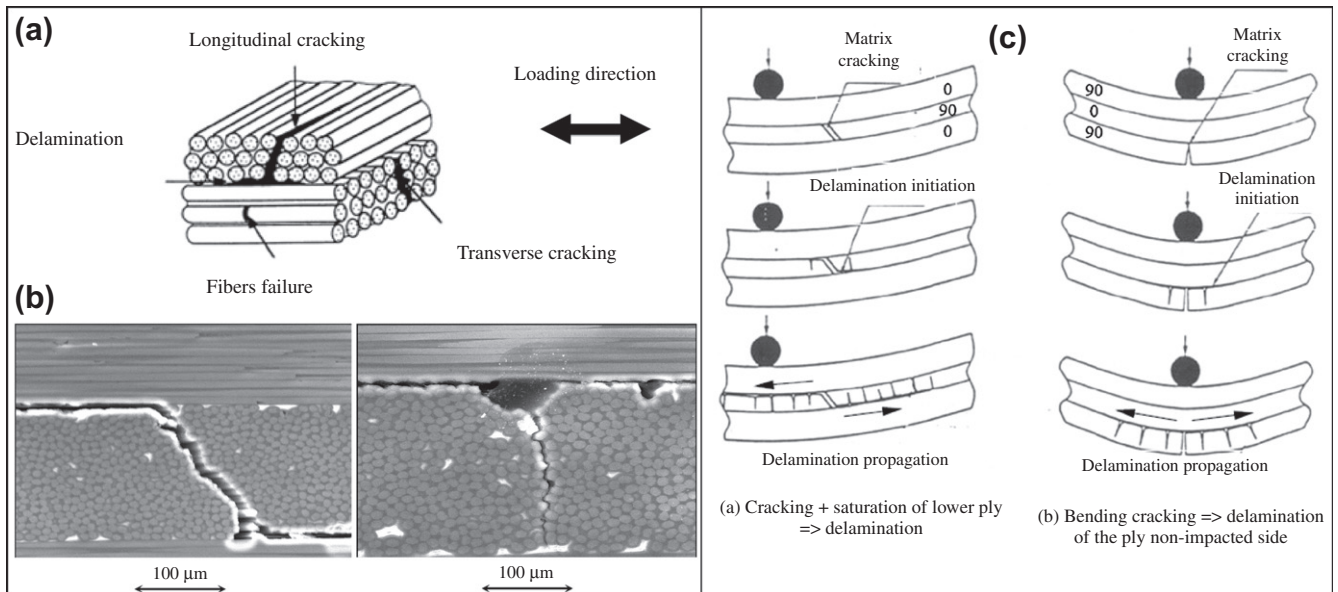


Fig. 3. Impact damage in laminate with UD reinforcement: (a) different damage types [7], (b) damage photographs [5], and (c) diagram of the principle of interaction between intra- and inter-laminar damage [11].

## 2. Modeling principle

A low velocity/low energy impact on a composite laminate with UD reinforcement induces three types of damage: matrix cracks, fiber failure and delamination (Fig. 3) [5,7,11].

Conventionally, the first damage to appear is matrix cracking. When this damage increases, delamination quickly occurs. Interaction between these two damage phenomena is clearly visible during impact tests. This interaction is crucial to explain the very original morphology of the delaminated interfaces through the

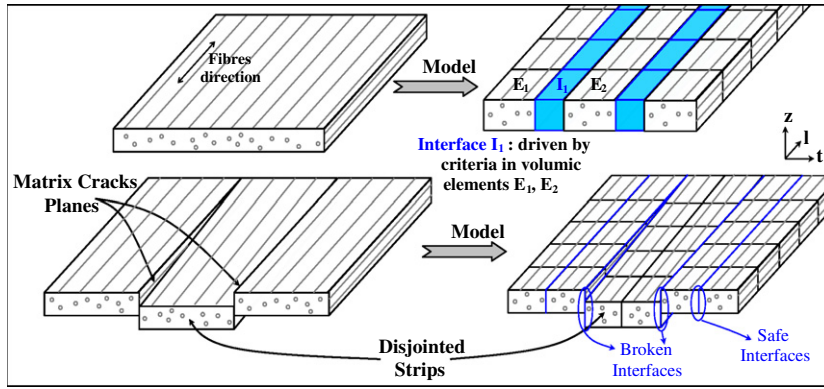


Fig. 4. Model of the ply with longitudinal strips.

thickness of the plate. Chang and Chang illustrate this interaction [11] in Fig. 3c which schematically shows the two types of delamination formation:

- The delamination induced by inner shear cracks which generates a substantial delamination along the bottom interface and a small confined delamination along the upper interface of the cracked plies.
- The delamination induced by a surface bending crack, which generates a delamination along the first interface of the cracked ply.

Consequently, the key point for an impact model is the interaction between intra-laminar damage, namely matrix cracks and fiber failure, and inter-laminar damage, namely delamination. Some models in the literature (e.g. [8–10,17,26]) take this interaction into account using explicit relations between the damage variables of matrix cracking in the ply and the damage variables of delamination between plies. Another way to model this interaction is to allow for the discontinuity created by matrix cracks, in order to naturally account for this interaction [8,27]. Indeed, this discontinuity seems essential for the formation of the impact damage [28] and should be modeled to correctly simulate this damage morphology. Consequently, the plies mesh must respect the material orthotropy in order to account for the discontinuity aspect of the matrix cracks in the fiber direction. Then, in the proposed model, each ply is meshed separately using little longitudinal strips with one volume element in the ply thickness (Fig. 4).

### 2.1. Matrix cracking modeling

Afterwards, these little strips are connected together with zero-thickness interface elements normal to the transverse direction. These interface elements can account for matrix cracks in the thickness of the ply. Nevertheless, this type of mesh presents some drawbacks:

- This mesh is complicated by uniform size in the impact zone. Nevertheless, it is possible to simulate an impact on a real structure using a multi-scale approach: the model described above for the area concerned with impact damage, and a conventional FE model for the remaining structure [29].
- This mesh can only simulate cracks occurring through the entire thickness of the ply and is not able to simulate small, diffusive matrix cracks. This means the propagation of matrix cracks within the ply thickness is assumed to be instantaneous. Thus, if the ply thickness is not too great,

the propagation of a matrix crack in the thickness takes place very quickly and its effect on the creation of the impact damage should remain local.

- This mesh can only simulate cracks normal to interfaces. However, matrix cracks due to out-of-plane shear stress ( $\tau_{xz}$ ), are globally inclined at 45°. This hypothesis avoids the use of an overly complex mesh, and seems reasonable if the ply thickness is small compared to the laminate thickness.
- The mesh size imposes the maximum density of matrix cracks in the transverse direction of the ply. This drawback could seem very significant but the presence of one matrix crack, i.e. of a broken interface, should unload the neighboring interfaces in the transverse direction and prevent their breaking. Indeed, the matrix cracks, taken into account in this model, are only the largest ones, i.e. those running through the entire ply thickness, and not the little, diffuse matrix cracks. This means that the model does not take into account the network of little matrix cracks because the effect of these diffuse matrix cracks seems small compared to those running through the entire thickness.

Another consequence of this imposed maximum density of matrix cracks is the choice of the failure criterion and energy dissipated by this phenomenon. It would be interesting to use fracture mechanics, in addition to interface elements, to simulate the critical energy release rate [30]. But the mesh density is imposed a priori and induces the maximum energy possible to dissipate, unless the mesh is fine enough to simulate each crack. As it is not possible to simulate each matrix crack (Fig. 2a), the proposed model has been chosen without energy dissipation.

Then the model ignores the energy dissipated by matrix cracking, even if a part of this energy should be included in the energy dissipated by delamination. Indeed, the DCB (Double Cantilever Beam) test, which is used to evaluate the critical energy release rate for delamination, is a overall test. In practical terms, the energy dissipated during the test which is experimentally evaluated, is the sum of all damage types [31,32]. In particular, the energy dissipated by the matrix cracks, accompanying the delamination, is taken into account. Nevertheless, the consequences of this non-dissipative model should be evaluated with other experimental tests. Another solution would be to use cohesive crack modeling to allow multiple matrix cracks per element, as proposed by Raimondo et al. [33].

In the proposed case, the interface degradation is abrupt: if the material is safe, the stiffness of these matrix cracking interfaces is considered to be very high (typically  $10^6$  MPa/mm) and this stiffness is set to zero if matrix cracks exist. Of course, this abrupt

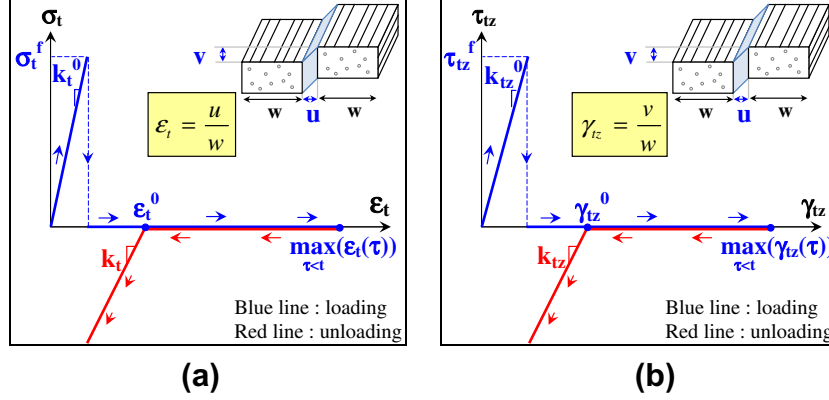


Fig. 5. Permanent indentation model under tension (a) and shear (b).

degradation can induce shock issue during numerical simulation and additional damping should be added [22]. The energy dissipated by this viscosity damping should remain low [34], typically less than 2% of the total energy.

The failure is driven by a standard criterion similar to Hashin's criterion [35,36], calculated in the neighboring volume elements:

$$\left(\frac{\langle \sigma_t \rangle^+}{\sigma_t^f}\right)^2 + \frac{\tau_{lt}^2 + \tau_{tz}^2}{(\tau_{lt}^f)^2} \leq 1 \quad (2)$$

where  $\sigma_t$  is the transverse stress,  $\tau_{lt}$  and  $\tau_{tz}$  the shear stresses in the ( $lt$ ) and ( $tz$ ) planes,  $\langle \cdot \rangle^+$  the positive value,  $\sigma_t^f$  the transverse failure stress and  $\tau_{lt}^f$  the shear failure stress of the ply. This conventional quadratic criterion [35,36] is written with stresses at each Gauss point of the two neighboring volume elements and the interface is broken when the criterion is reached at one of these points (for more details, see [24]). This is an original point of the proposed model and can be considered to be an average stress over a distance which depends on the mesh size. This mesh sensitivity will have to be studied further; this work is currently in progress.

Hereafter, these matrix cracking interface elements are used to simulate permanent indentation. Indeed, part of the permanent indentation seems to be impact debris in 45° cracks through the ply thickness (Fig. 2) [12]. This phenomenon has been taken into account in the present model using an original "plastic-like" model behavior in the matrix cracking elements in order to limit their closure after failure under tension ( $\sigma_t$ ) and out-of-plane shear ( $\tau_{tz}$ ) (Fig. 5). The formulation of the law after crack initiation is given below:

$$\begin{cases} \varepsilon_t \geq \min\left(\max_{\tau \leq t}(\varepsilon_t(\tau)), \varepsilon_t^0\right) \Rightarrow \sigma_t = 0 \\ \varepsilon_t < \min\left(\max_{\tau \leq t}(\varepsilon_t(\tau)), \varepsilon_t^0\right) \Rightarrow \sigma_t = k_t \cdot \left(\varepsilon_t - \min\left(\max_{\tau \leq t}(\varepsilon_t(\tau)), \varepsilon_t^0\right)\right) \\ \gamma_{tz} \geq \min\left(\max_{\tau \leq t}(\gamma_{tz}(\tau)), \gamma_{tz}^0\right) \Rightarrow \tau_{tz} = 0 \\ \gamma_{tz} < \min\left(\max_{\tau \leq t}(\gamma_{tz}(\tau)), \gamma_{tz}^0\right) \Rightarrow \tau_{tz} = k_{tz} \cdot \left(\gamma_{tz} - \min\left(\max_{\tau \leq t}(\gamma_{tz}(\tau)), \gamma_{tz}^0\right)\right) \end{cases} \quad (3)$$

where  $k_t$  and  $k_{tz}$  are the stiffness values of debris,  $\varepsilon_t$  and  $\gamma_{tz}$  are the dimensionless displacements of the interface displacements, and  $\varepsilon_t^0$  and  $\gamma_{tz}^0$  the dimensionless sizes (Fig. 5) of these debris respectively in the normal direction and in shear:

$$\begin{cases} \varepsilon_t = \frac{u}{w} \\ \gamma_{tz} = \frac{v}{w} \end{cases} \quad - \quad \begin{cases} \varepsilon_t^0 = \frac{u^0}{w} \\ \gamma_{tz}^0 = \frac{v^0}{w} \end{cases} \quad (4)$$

where  $w$  is the width of the element and  $u^0$  and  $v^0$  are the sizes of the debris respectively in the normal and transverse direction (Fig. 5).

Then, when a matrix crack exists, its closure is prevented if its dimensionless displacement  $\varepsilon_t$  ( $\gamma_{tz}$ ) is below a critical size  $\varepsilon_t^0$  ( $\gamma_{tz}^0$ ) corresponding to the debris size. This critical debris size can be compared to the critical indentation  $\alpha_{cr}$  (Eq. (1)) proposed by Karakuzu et al. [21].

If the crack is assumed to be 45° in the ( $tz$ ) plane these two stiffness values and debris sizes are equivalent and are assumed to be equal:

$$k_t = k_{tz} \quad - \quad \varepsilon_t^0 = \gamma_{tz}^0 \quad (5)$$

Consequently, only two material parameters are necessary to take into account the phenomenon of permanent indentation. These two parameters are difficult to correlate with material parameters measured in conventional tests and are directly determined using the impact test. Therefore, this evaluation process limits the predictive character of this model, and in particular for the part linked to permanent indentation. Other works are in progress to evaluate these parameters using simpler experimental studies. It can be observed that these two parameters are the only ones in this model which are directly determined during the impact test: all other values are obtained from conventional experimental tests described in the literature [31,32,37,38,41].

This no-closure model integrated into the interface elements of matrix cracking makes it possible to obtain a realistic deformed shape of the plate, not only during impact but also after impact, as well as a permanent indentation (Fig. 14).

## 2.2. Fiber failure modeling

For the fiber failures observed after impact (Fig. 2), there is no evidence of distributed fiber damage. Moreover, due to the high critical energy release rate of fiber failure [38], it is necessary to dissipate this energy in the model. Additional interface elements could be used but would result in very complex meshing. Therefore, to avoid the use of such interfaces, fiber failure is taken into account using conventional continuum damage mechanics with original formulation to produce a constant energy release rate per unit area. This approach can be compared to methods based on characteristic element length, which makes mesh-size independent modeling possible [15,35,39,40].

Therefore, in order to simulate the critical energy release rate due to fiber failure per unit area of crack, the dissipated energy of a volume element should be:

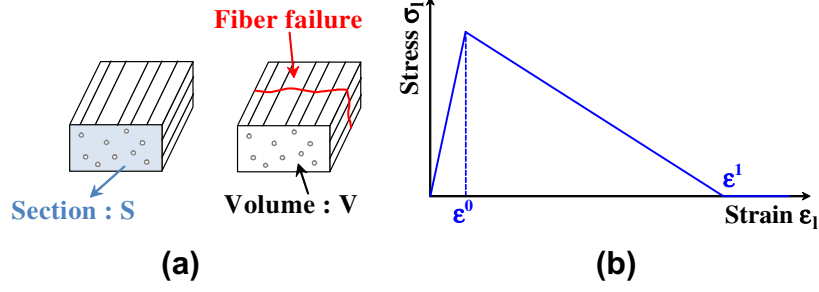


Fig. 6. Principle of fiber failure (a) and behavior law in the longitudinal direction (b).

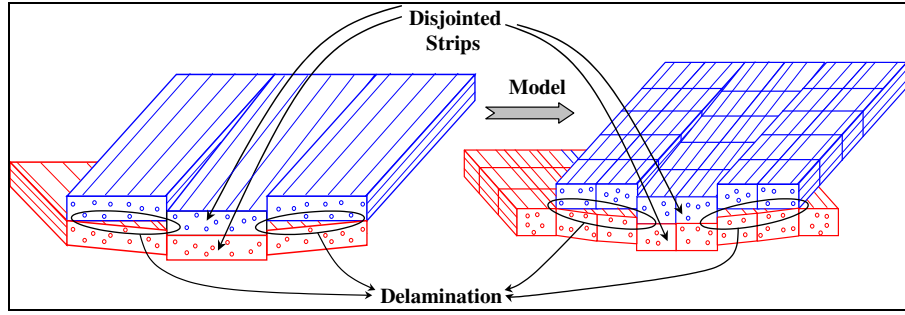


Fig. 7. Principle of the interface model between plies.

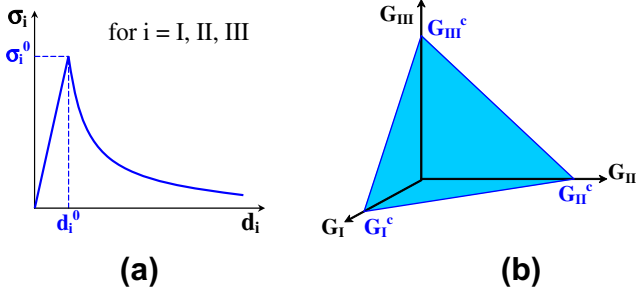


Fig. 8. Evolution of the stress–relative displacement jump curves (a) and linear mixed mode of fracture (b).

$$\int_V \left( \int_0^{\varepsilon^1} \sigma_l \cdot d\varepsilon_l \right) \cdot dV = S \cdot G_I^f \quad (6)$$

where  $\varepsilon_l$  ( $\sigma_l$ ) is the longitudinal stress (strain),  $V(S)$  the volume (section) of the element,  $\varepsilon^1$  is the strain of total degradation of the fiber stiffness (Fig. 6) and  $G_I^f$  the energy release rate in opening mode I (Fig. 6), but could be generalized with other fracture modes.

Afterwards, the stiffness in fibers is degraded using a damage variable  $d_f$ :

$$\sigma_l = (1 - d_f) \cdot (H_{ll} \cdot \varepsilon_l + H_{lt} \cdot \varepsilon_t + H_{lz} \cdot \varepsilon_z) \quad (7)$$

where  $H_{ll}$ ,  $H_{lt}$  and  $H_{lz}$  are the stiffness values in the longitudinal direction. And this damage variable is conventionally calculated according to the longitudinal strain in order to obtain a linear decrease of the longitudinal stress (Fig. 6) [15]:

$$d_f = \frac{\varepsilon^1 \cdot (\varepsilon_l - \varepsilon^0)}{\varepsilon_l \cdot (\varepsilon^1 - \varepsilon^0)} \quad (8)$$

where  $\varepsilon^1$  is calculated using Eq. (6) and  $\varepsilon^0$  is the strain of damage initiation.

An originality of this fiber failure approach is to initiate the damage when the maximum of the longitudinal strains calculated at the element nodes reaches the fiber failure strain  $\varepsilon_f^1$ . The use of extrapolated strains at element nodes, rather than direct strain values at integration points, makes it easier to take into account the bending behavior of each ply with only one finite volume element in the thickness. Nevertheless, this condition prevents the use of reduced integration elements and involves the use of eight Gauss points elements. Then, the  $\varepsilon^0$  parameter is common to the eight Gauss points of each element and is evaluated using the longitudinal strains calculated at the element nodes. The  $\varepsilon^1$  and  $d_f$  parameters are also chosen common to the eight Gauss points in order to solve the Eq. (6) only one time for each element.

### 2.3. Delamination modeling

After the different plies are meshed with volume elements and matrix crack interface elements (Fig. 4), two consecutive plies are joined using zero-thickness interface elements (Fig. 7).

These delamination interface elements are conventionally softening interfaces [30,42] of zero thickness, driven by fracture mechanics. They are written in mixed fracture mode (modes I, II, III) to simulate the energy dissipated by delamination. Moreover, the shearing (II) and tearing (III) fracture modes are combined and in the following, the term of mode II will be abusively used to name fracture modes II and III. Then, an equivalent relative displacement jump is written in order to simulate a linear coupling law between the fracture modes:

$$d_{eq} = \sqrt{((d_I)^+)^2 + \left(\frac{d_I^0}{d_{II}^0} \cdot d_{II}\right)^2 + \left(\frac{d_I^0}{d_{III}^0} \cdot d_{III}\right)^2} \quad (9)$$

where  $d_I$ ,  $d_{II}$  and  $d_{III}$  are the relative displacement jumps respectively in the  $z$ ,  $l$  and  $t$  directions,  $d_I^0$ ,  $d_{II}^0$  and  $d_{III}^0$  are the critical relative displacement jumps respectively in the  $z$ ,  $l$  and  $t$  directions



**Table 1**  
Material parameters.

$E_l^i$ (GPa)	$E_t^i$ (GPa)	$E_z$ (GPa)	$\nu_{lt}$	$G_{lt}$ (GPa)	$\sigma_t^f$ (MPa)	$\tau_{lt}^f$ (MPa)
130	100	10	0.29	4.8	50	90
$k_l^0$ (MPa/mm)	$e_l^f$	$G_{ll}^d$ (N/mm)	$G_{tt}^d$ (N/mm)	$G_{ll}^f$ (N/mm)	$e_z^0$	$k_t$ (MPa/mm)
$10^6$	0.016	0.5	1.6	133	0.02	10000

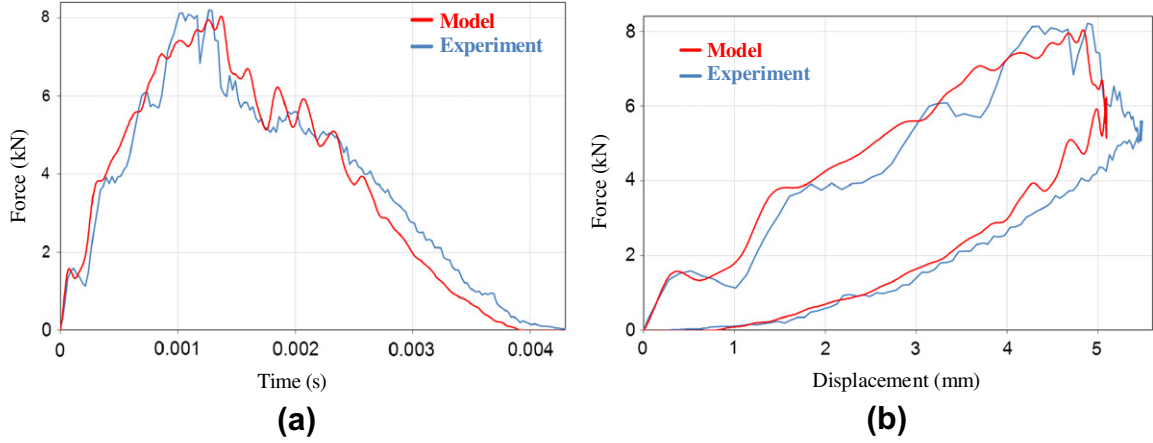


**Fig. 9.** Curves of force versus time (a) and displacement (b) obtained experimentally and numerically.

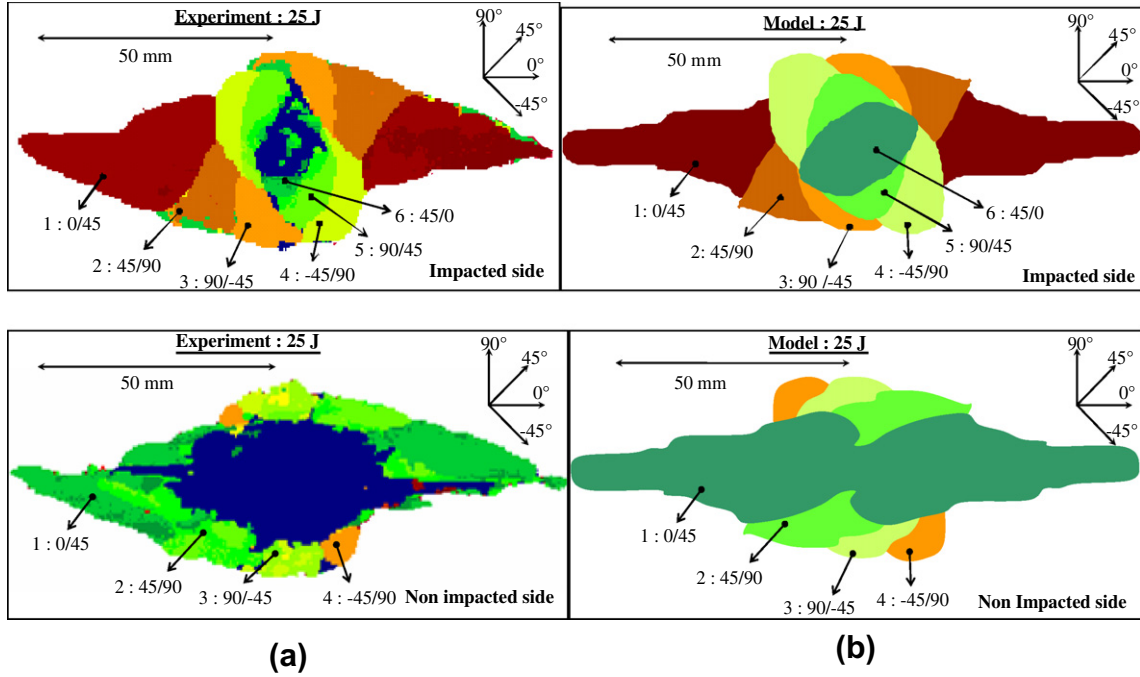


**Fig. 10.** Comparison between delaminated interfaces obtained experimentally (a) and numerically (b) after a 25-J impact test.

calculated according to failure stresses (Fig. 8) (for more details, see [25]):

$$d_l^0 = \frac{\sigma_l^0}{k_l^0} \quad - \quad d_{ll}^0 = \frac{\sigma_{ll}^0}{k_{ll}^0} \quad - \quad d_{lll}^0 = \frac{\sigma_{lll}^0}{k_{lll}^0} \quad (10)$$

where  $k_l^0$ ,  $k_{ll}^0$  and  $k_{lll}^0$  are the stiffness values respectively in the  $z$ ,  $l$  and  $t$  directions and  $\sigma_l^0$ ,  $\sigma_{ll}^0$  and  $\sigma_{lll}^0$  are the critical stresses

respectively in the  $z$ ,  $l$  and  $t$  directions. And the two shear directions are assumed to be equivalent:

$$d_{lll}^0 = d_{ll}^0 \quad - \quad k_{lll}^0 = k_{ll}^0 \quad - \quad \sigma_{lll}^0 = \sigma_{ll}^0 \quad (11)$$

To avoid introducing additional material parameters, the critical stresses are assumed to be equal to the failure stresses of the ply:

$$\sigma_l^0 = \sigma_t^f \quad - \quad \sigma_{ll}^0 = \sigma_{lll}^0 = \tau_{lt}^f \quad (12)$$

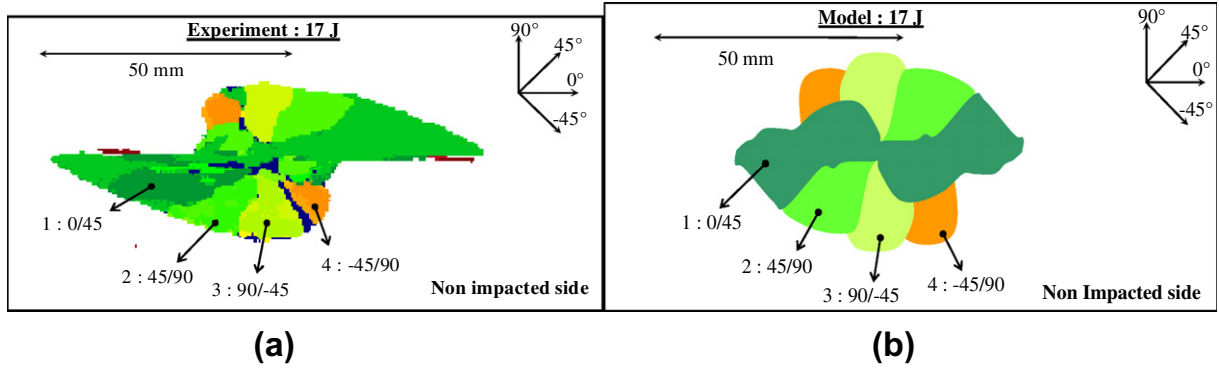


Fig. 11. Comparison between delaminated interfaces obtained experimentally (a) and numerically (b) after a 17-J impact test.

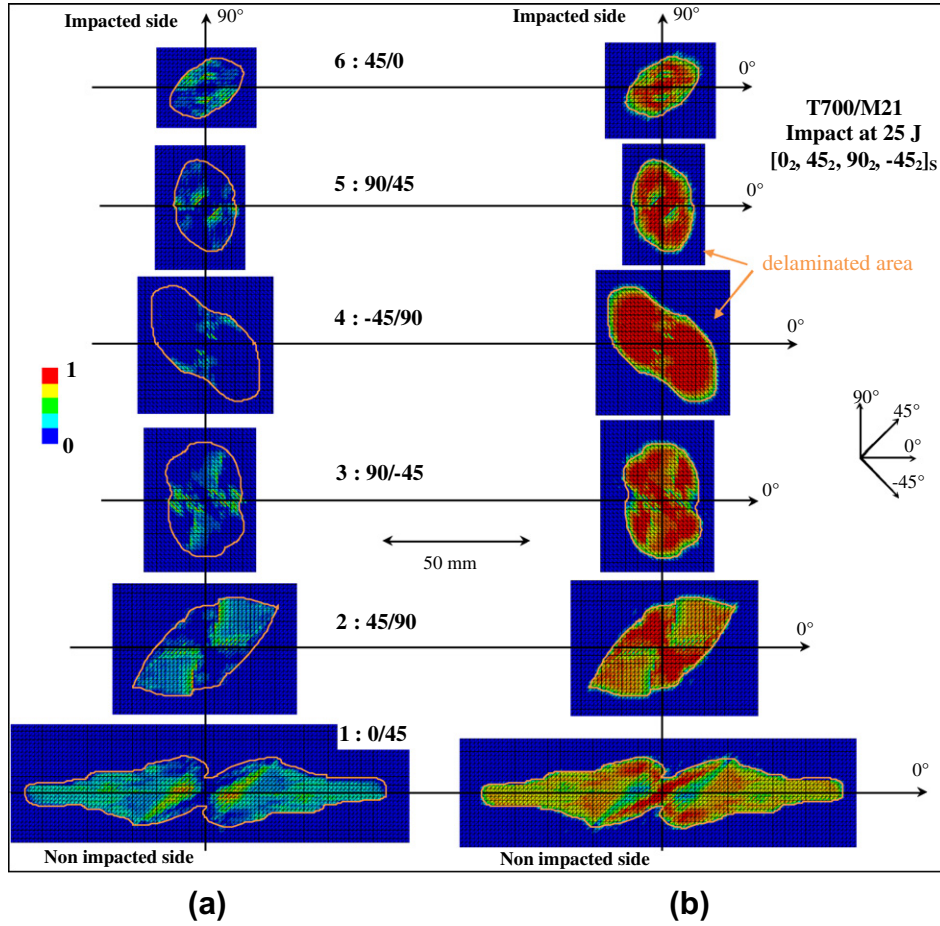


Fig. 12. Dimensionless energy release rates in mode I,  $G_I/G_I^d$  (a), and mode II,  $G_{II}/G_{II}^d$  (b) for each interface.

Then, a decreasing exponential law is chosen:

$$\begin{cases} \sigma_I = \sigma_I^0 \cdot \exp\left(-\beta \cdot (d_{eq} - d_I^0)\right) \frac{d_I}{d_{eq}} \\ \sigma_{II} = \sigma_{II}^0 \cdot \exp\left(-\beta \cdot (d_{eq} - d_{II}^0)\right) \frac{d_{II}}{d_{eq}} \frac{d_I^0}{d_{II}^0} \\ \sigma_{III} = \sigma_{III}^0 \cdot \exp\left(-\beta \cdot (d_{eq} - d_{III}^0)\right) \frac{d_{III}}{d_{eq}} \frac{d_I^0}{d_{III}^0} \end{cases} \quad (13)$$

where the coefficient  $\beta$  is determined to dissipate the energy release rate  $G_I^d$  in mode I under the stress-strain curve and  $G_{II}^d$  in mode II and III (Fig. 8):

$$\beta = \frac{1}{\frac{G_I^d}{\sigma_I^0} - \frac{d_I^0}{2}} \quad (14)$$

And the use of the same  $\beta$  coefficient for modes I, II and III imposes:

$$k_{II}^0 = k_{III}^0 = \frac{(\sigma_{II}^0)^2}{G_{II}^d} \left( \frac{1}{2} + \frac{1}{\beta \cdot d_I^0} \right) \quad (15)$$

The last undetermined coefficient  $k_I^0$  (Table 1) is considered to be very high. It can be observed that a linear mixed mode of fracture is imposed (Fig. 8b) due to the choice of the equivalent relative displacement jump (Eq. (9)).

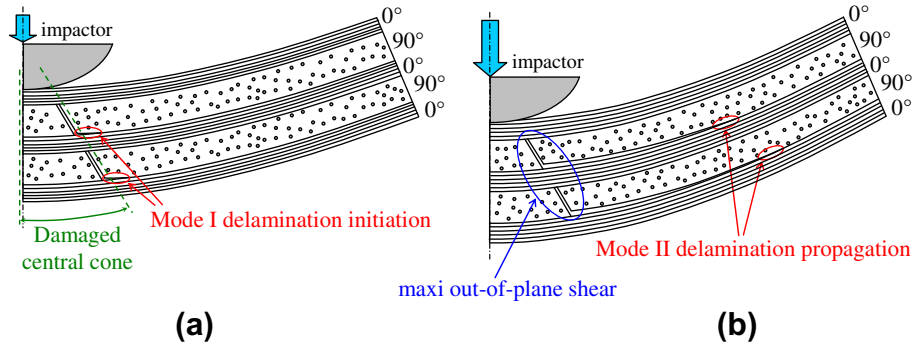


Fig. 13. Impact damage with creation of a highly damaged central conical shape: delamination initiation in mode I (a) and propagation in mode II (b).

This model adopted for delamination is often used in the literature [8,28] although this expression (Eq. (9)) is original. The definition of this equivalent relative displacement jump enables us to automatically compare all the possible mode ratios and how much energy should still be available to dissipate until total failure occurs. Indeed, during complex loading, with large variation in the mode ratio, it is not very easy to evaluate this remaining energy to be dissipated using conventional formulation [30,41].

### 3. Experimental validations

The proposed model is used to simulate an experimental impact test on a  $100 \times 150 \text{ mm}^2$  laminate plate manufactured with T700/M21 carbon/epoxy composite with UD reinforcement. This plate, with stacking sequence  $[0_2, 45_2, 90_2, -45_2]_S$  is simply supported by a  $75 \times 125 \text{ mm}^2$  window (AITM 00-10) and impacted at 25 J with a 16 mm diameter 2 kg impactor. Only half of the plate is meshed due to symmetry considerations, the boundary conditions are imposed to represent the contact with a fixed rigid body and the impactor is assumed to be non-deformable. The mechanical characteristics of this material and the material parameters used in this model are summarized in Table 1.

In this table (Table 1),  $E_f^t$  ( $E_f^c$ ) is the tension (compression) Young's modulus in the fiber direction,  $E_t$  is the Young's modulus in transverse direction,  $\nu_{ft}$  is the Poisson's ratio,  $G_{ft}$  is the shear modulus. As mentioned above (Section 2.1), it can be observed that the  $e_f^c$  and  $k_f$  are the only two parameters directly determined using the impact test: all other values come from conventional experimental tests presented in the literature [31,32,37,38,41].

The model is simulated using ABAQUS/Explicit® v6.9 with user subroutine Vumat. The total calculation time of this model is approximately 6 h with eight CPUs without optimization of the modeling to decrease this time.

The comparisons between experimental and numerical curves of impact force versus time and impactor displacement are illustrated in Fig. 9. A good correlation is obtained between the experiment and model, demonstrating that the real impact damage is well accounted for in the numerical simulation.

In Fig. 10, delaminated interfaces obtained by calculation are compared to the experimentally obtained results on the impacted and non-impacted sides. The accurate correlation between experimental and numerical results tends to confirm the relevance of the model, and in particular the model of interaction between inter and intra-laminar damage. As mentioned above (Section 2), the shape of the delaminations is closely linked to the interaction between matrix cracks and delamination. In particular, the orientation of delamination with the fibers of the lower ply or the characteristic shape of the first interface of the non-impacted side is accurately simulated. Moreover, this first delamination shape

seems to be nearly separated into two parts, just as in the experimental results, although in the C-scan, the extensive matrix cracking of the first ply of the non-impacted side makes this observation difficult. To confirm this result, which is coherent with the literature [1,9], a comparison was performed between the delamination and the C-scan examination performed on the non-impacted side of a 17-J impact (Fig. 11). This delamination shape can be explained by the creation of a central conical shape at the beginning of the impact test below the impactor, with high matrix cracking due to out-of-plane stresses ( $\tau_{tz}$  and  $\tau_{tz}$ ). The delamination tends to occur on the boundaries of this cone and is not created just below the impactor.

This phenomenon can be highlighted by the illustration of the dimensionless energy release rates in mode I,  $G_I/G_I^d$  and II,  $G_{II}/G_{II}^d$  at the end of the impact for each delaminated interface (Fig. 12). In this figure, blue<sup>1</sup> (resp. red) color corresponds to dimensionless energy release rate equals 0 (resp. 1) and the orange line to the mark of the delaminated area. It can be observed in this figure that mode II generally predominates compared to mode I, except in a central zone around the impactor point. This zone can be assimilated to a conical central zone with its axis in the impact direction and with its higher diameter on the non-impacted side. It can be concluded that at the beginning of the impact test, the direct contact of the impactor with the laminate induces a conical shape with high matrix cracking due to out-of-plane stresses ( $\tau_{tz}$  and  $\tau_{tz}$ ). These matrix cracks tend to isolate a central cone which induces the beginning of delamination with a high rate of mode I (Fig. 13a). This scenario is coherent with the literature [1,9], which indicates a precursor role regarding the development of delamination and which assumes that the delamination initiation is principally related to mode I characteristics.

After this phase of delamination initiation, propagation of delamination is principally defined by mode II (Fig. 13b). This shearing fracture mode is due to high stresses in the lower ply of the interface in the fiber direction ( $\sigma_f$ ), inducing high shear stresses in interfaces ( $\tau_{tz}$  and  $\tau_{tz}$ ), and explains the propagation direction of the delamination in the fiber direction of the lower ply.

In Fig. 14, the deformed shape of the plate, obtained numerically, is represented in two cut planes  $0^\circ$  and  $90^\circ$ , at maximum displacement (Fig. 14a) and after a 25-J impact (Fig. 14b). Some major damage is clearly visible in this figure: for example, the first ply, non-impacted side, is clearly broken in the transverse direction, which is visible in the  $90^\circ$  cut. It can also be observed that, for an impact of 25 J, this ply is not broken in the fiber direction. This transverse crack corresponds to the conventional crack observed after impact on the non-impacted side [27]. Delamination is also

<sup>1</sup> For interpretation of color in Figs. 12 and 15, the reader is referred to the web version of this article.

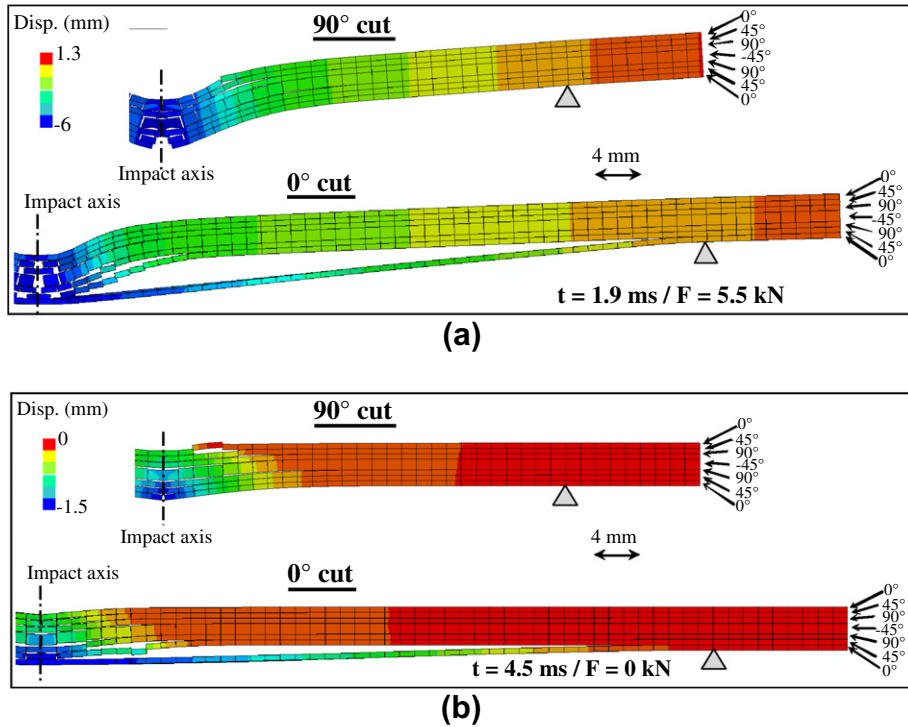


Fig. 14. Deformed mesh during 25 J impact at maximum displacement (a) and after impact (b).

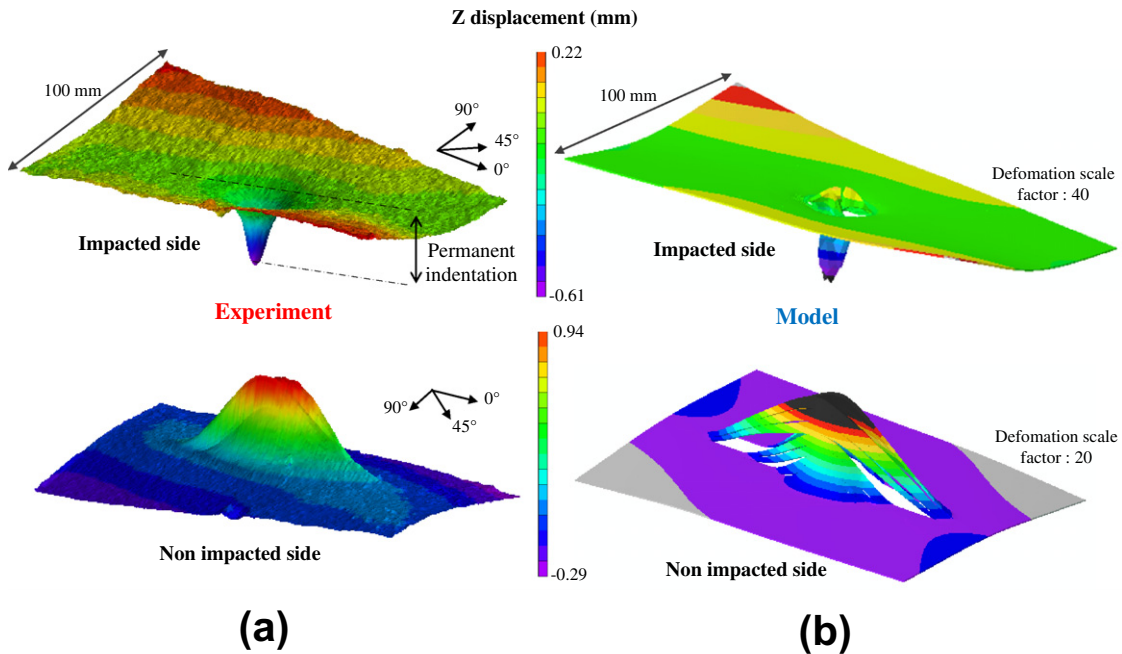


Fig. 15. Deformed shape of the plate after a 25 J impact: experimental (a) and numerical (b) results.

observable, in the very large opening of the first interface, non-impacted side, on the 0° cut. The significant delamination of this interface is conventionally observed using C-Scan (Fig. 10a). The central zone below the impactor is also severely damaged, as in the experiment (Fig. 2a). The overall simulated shape of permanent deformation (Fig. 10b) correlates well with experimental photographs (Fig. 2a) and in particular the permanent opening of the non-impacted side's first delamination is obtained, although the simulated opening is larger than the experimental one. This difference can be partially due to the experimental procedure of cutting

and polishing which induces partial disappearance of the permanent indentation, but also to the model of matrix crack blocking which is in an early stage and should be confirmed in other cases. A study is currently underway to determine the importance of debris blocking of the 45° cracks on the permanent indentation.

Then, the deformed shape of the plate resulting from the 25-J impact is plotted on the impacted and non-impacted sides (Fig. 15). The experimental results are obtained with Vic-3D® image correlations and the numerical results are obtained from the finite element calculations. The permanent indentation is

clearly visible on the impacted side, but is difficult to define because the plate is twisted. We choose to define it according to the distance between the lowest line of the twisted plate and the lowest point of the plate, i.e. at the impact point (Fig. 15a). In this case, a value of about 0.5 mm is obtained. The plate shape after impact is accurately simulated by the numerical model, and in particular, the general twisted shape of the plate is reproduced. The orientation of the twisted shape, in the diagonal the nearest to the 45° ply, is due to the  $[0_2, 45_2, 90_2, -45_2]_S$  draping sequence which induces a higher bending stiffness in this direction. In practical terms, the bending stiffness in this direction. In practical terms, the bending stiffness  $D_{11}$  is about  $3.6 \times 10^5$  N. mm in the 45° direction, compared to  $1.8 \times 10^5$  N. mm in the -45° direction.

This twisted shape is also visible on the non-impacted side, in both the experimental and numerical results. Moreover, the deformation of the impact point is larger than on the impacted side. For example, in the Z direction, the permanent indentation is about 1 mm compared to 0.5 mm on the impacted side. On the non-impacted side, the terms of the impact point and the permanent indentation have been exaggerated to simplify the discussion. This higher indentation on the non-impacted side is due to the increased plate thickness in the impacted zone. This phenomenon is also visible in the micrographic cuts (Fig. 2), although it is lower, probably due to the cutting and polishing processes. It is generally simulated by the model, although amplified. Indeed, the black zone (Fig. 15b) represents Z-displacements above 0.94 mm, the highest experimental value, and the gray zone represents Z-displacements below -0.29 mm, the lowest experimental value obtained. Moreover, the experimental and numerical scales are set to a constant and were correlated to half scale (green color). Moreover, it can be observed on the numerically obtained, non-impacted side of the deformed shape, openings exist between consecutive fiber strips (white colored zone). These opening are artificial and due to the large deformation scale factor.

The deformed zone is also larger in the 0° plane of the non-impacted side, compared to the impacted side. This phenomenon is also generally simulated by modeling even if it is amplified. Consequently, the relatively good correlation of the simulations with experimental results on the deformed shape obtained after impact shows the accuracy of the permanent indentation modeling.

#### 4. Conclusion

A numerical model has been elaborated in order to simulate the different impact damage types developing during low velocity/low energy impact. The three most current damage types are simulated: matrix cracking, fiber failure and delamination.

The originality of the proposed model is to simulate permanent indentation after impact with a “plastic-like” model introduced in the interface elements of matrix cracking. This choice is based on experimental observations showing matrix cracking debris which block crack closure. The accurate correlation between experimental and numerical results, in particular of the deformation after impact, confirms the interest of this novel approach in describing the physics behind permanent indentation. Nevertheless, modeling the permanent indentation required two supplementary material parameters. These parameters are difficult to relate to conventional material parameters measured in conventional tests and are directly determined using the impact test. Therefore, this evaluation process limits the predictive character of this model, and in particular for the part linked to permanent indentation. Other studies are currently underway in order to evaluate these parameters with other, simpler experimental studies.

This model accurately simulates a reference impact case on composite laminate with UD reinforcement with a few material

parameters to identify. Indeed, except for the two material parameters for permanent indentation directly determined using impact tests, all other values are obtained from conventional experimental tests described in the literature. Of course, this conclusion should be confirmed with other conditions, such as other impact energies, other draping sequences, other boundary conditions, and other materials. Moreover, the mesh sensitivity should be studied further.

This modeling results in very complex meshing with many elements and a long calculation time. This is a problem for industrial calculation with complex draping sequences and complex geometry. Nevertheless, it is possible to simulate an impact on a real structure using this type of model for the area concerned with the impact damage, and with a classical FE model on the remaining structure.

Lastly, in order to be able to numerically optimize design of composite structures with impact damage tolerance, it is necessary to simulate the impact damage and the residual mechanical characteristics after impact, using the same model. This work is currently in progress and shows that other problems appear, for example, fiber failure under compression stress.

#### References

- [1] Abrate S. Impact on composites structures. Cambridge Univ. Press; 1998.
- [2] Rouchon J. Fatigue and damage tolerance aspects for composite aircraft structures. Delft; 1995.
- [3] Tropis A, Thomas M, Bounie JL, Lafon P. Certification of the composite outer wing of the ATR72. *J Aero Eng* 1994;209:327–39.
- [4] Alderliesten RC. Damage tolerance of bonded aircraft structures. *Int J Fatigue* 2008;31(6):1024–30.
- [5] Petit S, Bouvet C, Bergerot A, Barrau JJ. Impact and compression after impact experimental study of a composite laminate with a cork thermal shield. *Compos Sci Technol* 2007;67:3286–99.
- [6] Zheng D, Binienda WK. Effect of permanent indentation on the delamination threshold for small mass impact on plates. *Int J Solid Struct* 2007;44(25–26):8143–58.
- [7] Eve O. Etude du comportement des structures composites endommagées par un impact basse vitesse. Thèse de doctorat. Université de Metz; 1999.
- [8] Allix O, Blanchard L. Mesomodeling of delamination: towards industrial applications. *Compos Sci Technol* 2006;66:731–44.
- [9] Choi HY, Chang K. A model for predicting damage in graphite/epoxy laminated composites resulting from low-velocity point impact. *J Compos Mater* 1992;26(14):2134–69.
- [10] De Moura MF, Gonçalves SF. Modelling the interaction between matrix cracking and delamination in carbon-epoxy laminates under low velocity impact. *Compos Sci Technol* 2004;64:1021–7.
- [11] Chang FK, Chang K. A progressive damage model for laminate composites containing stress concentrations. *J Compos Mater* 1987;834–55.
- [12] Abi Abdallah E, Bouvet C, Rivallant S, Broll B, Barrau JJ. Experimental analysis of damage creation and permanent indentation on highly oriented plates. *Compos Sci Technol* 2009;69(7–8):1238–45.
- [13] Chen P, Shen Z, Xiong J, Yang S, Fu S, Ye L. Failure mechanisms of laminated composites subjected to static indentation. *Compos Struct* 2006;75:489–95.
- [14] Caprino G, Langella A, Lopresto A. Indentation and penetration of carbon fibre reinforced plastic laminates. *Composites: Part B* 2003;34:319–25.
- [15] Shi Y, Swait T, Soutis C. Modelling damage evolution in composite laminates subjected to low velocity impact. *Compos Struct*; 2012. doi: 10.1016/j.compstruct.2012.03.039.
- [16] Fiedler B, Hojo M, Ochiai S, Schulte K, Ando M. Failure behavior of an epoxy matrix under different kinds of static loading. *Compos Sci Technol* 2001;61:1615–24.
- [17] Faggioli A, Falzon BG. Predicting low-velocity impact damage on a stiffened composite panel. *Composites: Part A* 2010;41(6):737–49.
- [18] Iannucci L, Willows ML. An energy based damage mechanics approach to modelling impact onto woven composite materials – Part I: Numerical models. *Composites: Part A* 2006;37:2041–56.
- [19] Johnson HE, Louca LA, Mouring S, Fallah AS. Modelling impact damage in marine composite panels. *Int J Imp Eng* 2009;36:25–39.
- [20] Berbinau P, Soutis C, Goutas P, Curtis PT. Effect of off-axis ply orientation on 0-fibre microbuckling. *Composites Part A* 1999;30:1197–207.
- [21] Karakuzu R, Erbil E, Aktas M. Impact characterization of glass/epoxy composite plates: an experimental and numerical study. *Composites Part B* 2010;41:388–95.
- [22] Gonzalez EV, Maim P, Camanho PP, Turon A, Mayugo JA. Simulation of drop-weight impact and compression after impact tests on composite laminates. *Comput Struct*; 2012. doi: 10.1016/j.compstruct.2012.05.015.

- [23] Donadon MV, Iannucci L, Falzon BG, Hodgkinson JM, de Almeida SFM. A progressive failure model for composite laminates subjected to low velocity impact damage. *Comput Struct* 2008;86(11–12):1232–52.
- [24] Bouvet C, Castanié B, Bizeul M, Barrau JJ. Low velocity impact modeling in laminate composite panels with discrete interface elements. *Int J Solid Struct* 2009;46(14–15):2809–21.
- [25] Bouvet C, Rivallant S, Barrau JJ. Low velocity impact modelling in laminate composites and permanent indentation. Workshop on dynamic failure of composites and sandwich structures. Toulouse, France: Institut Clément Ader; 2011.
- [26] Lopes CS, Camanho PP, Gürdal Z, Maimí P, González EV. Low-velocity impact damage on dispersed stacking sequence laminates. Part II: Numerical simulations. *Compos Sci Technol* 2009;69(7–8):937–47.
- [27] Aymerich F, Dore F, Priolo P. Simulation of multiple delaminations in impacted cross-ply laminates using a finite element model based on cohesive interface elements. *Compos Sci Technol* 2009;69:1699–709.
- [28] Wisnom MR. Modelling discrete failures in composites with interface elements. *Compos Part A: Appl Sci Manuf* 2010;41(7):795–805.
- [29] Ha-Minh C, Kanit T, Boussu F, Abdellatif I. Numerical multi-scale modeling for textile woven fabric against ballistic impact. *Compos Mater Sci* 2011;50(7):2172–84.
- [30] Mi Y, Crisfield MA, Davies GAO. Progressive delamination using interface elements. *J Compos Mater* 1998;32(14):1246–72.
- [31] Prombut P. Caractérisation de la propagation de délaminage des stratifiés composites multidirectionnels. Thèse de doctorat. Université de Toulouse; 2007.
- [32] Prombut P, Michel L, Lachaud F, Barrau JJ. Delamination of multidirectional composite laminates at  $0^\circ/\theta^\circ$  ply interfaces. *Eng Fract Mech* 2006;7:2427–42.
- [33] Raimondo L, Iannucci L, Robinson P, Curtis PT. A progressive failure model for mesh-size-independent FE analysis of composite laminates subject to low-velocity impact damage. *Compos Sci Technol* 2012;72:624–32.
- [34] ABAQUS 6.9-3 User's manual. (RI) USA: Dassault Systemes Simulia Corp. Providence; 2009.
- [35] Hashin Z, Rotem A. A fatigue failure criterion for fiber-reinforced materials. *J Compos Mater* 1973;7:448–64.
- [36] Hashin Z. Failure criteria for unidirectional fiber composites. *J Appl Mech* 1980;47:329–34.
- [37] Hexply<sup>®</sup> M21 product data – HexPly company.
- [38] Pinho ST, Robinson P, Iannucci L. Fracture toughness of the tensile and compressive fibre failure modes in laminated composites. *Compos Sci Technol* 2006;66:2069–79.
- [39] Caprino G, Lopresto A, Langella A, Leone C. Damage and energy absorption in GFRP laminates impacted at low-velocity: indentation model. *Proc Eng* 2011;10:2298–311.
- [40] Bazant ZP, Oh BH. Progressive Crack and band theory for fracture of concrete. *Mater. Struct.* 1983;16:155–77.
- [41] Pinho ST. Modelling failure of laminated composites using physically-based failure models. PhD of the University of London; 2005.
- [42] Yang Q, Cox B. Cohesive models for damage evolution in laminated composites. *Int J Fract* 2005;133:107–37.